

IJECBE (2025), 3, 3, 567–578 Received (19 May 2025) / Revised (30 June 2025) Accepted (2 July 2025) / Published (30 September 2025) https://doi.org/10.62146/ijecbe.v3i3.129 https://ijecbe.ui.ac.id ISSN 3026-5258

International Journal of Electrical, Computer and Biomedical Engineering

RESEARCH ARTICLE

Development of a 1550 nm LiDAR System Using Galvanometer and i-ToF Method for Distance Measurement and 2D Object Reconstruction

Febrian Winston Hutagalung[†], Mefina Yulias Rofianingrum[‡], Asep Hapiddin[¶], Dwi Hanto[‡], Sahat Pandapotan Nainggolan[§], and Retno Wigajatri Purnamaningsih^{*†}

†Opto-Electronics Laboratory, Department of Electrical Engineering, Faculty of Engineering, Universitas Indonesia, Depok, Indonesia

‡Research Center for Photonics, National Research and Innovation Agency, South Tangerang, Indonesia ¶Research Center for Testing Technology and Standard, National Research and Innovation Agency, South Tangerang, Indonesia

§Division of Mathematics and Physical Sciences, Graduate of Natural Science and Technology Kanazawa University, Japan

*Corresponding author. Email: retno.wigajatri@ui.ac.id

Abstract

LiDAR (Light Detection and Ranging) is a high-precision distance measurement technology based on laser light reflection. This study develops a galvanometer-based LiDAR system utilizing the indirect Time of Flight (i-ToF) method with 100 MHz sinusoidal modulation and a 1550 nm eye-safe laser diode. The system is designed to measure distance and identify the shape of 2D objects. The system was tested through phase difference measurements, galvanometer response, and flat-surface mapping at distances of 25 cm and 35 cm. This LiDAR system configuration produces linear and stable distance measurements under ideal conditions (galvanometer scanner reflection angle of 0°). A 1° phase difference change represents 4.2 mm (0.42 cm). With a Mean Absolute Error (MAE) of 0.06913 cm, Root Mean Squared Error (RMSE) of 0.09091 cm, and an average standard deviation (STD) of 0.07865 cm. The measurements of object dimensions in the form of an aluminum foil-covered plate at distances of 25 cm (1.76 cm × 2.63 cm) and 35 cm (2.45 cm × 3.66 cm) indicate that increasing the distance between the object and the system results in a wider coverage area but with reduced spatial resolution. At a distance of 25 cm the spatial resolution is 0.436 cm, and at a distance of 35cm, the spatial resolution is 0.611 cm. Furthermore, the limited active area of the photodetector was identified as the main factor restricting the detection coverage. This research opens opportunities for further development, particularly in optimizing galvanometer angle adjustments and

enhancing the photodetector's active area to expand coverage and improve measurement accuracy under various operating conditions.

Keywords: LiDAR, Object Identification, i-ToF, Galvanometer, Laser 1550 nm

1. INTRODUCTION

LiDAR (Light Detection and Ranging) is a technology capable of measuring object distances with high resolution and accuracy. It employs light or laser as the primary component for distance detection. In addition, LiDAR has been applied in various domains such as automotive applications [1], three-dimensional object mapping [2][3], robotics, drone-based area mapping [4][5], underwater object imaging [6], autonomous vehicle technologies [7], and the healthcare sector [8]. With ongoing technological advancements, LiDAR systems have evolved through the implementation of various fundamental methods for distance measurement. One of the most common techniques is Pulsed Time-of-Flight (ToF), which calculates distance based on the time interval between the emitted light pulse and the reflected signal received by the sensor. Another approach is the Amplitude Modulated Continuous Wave (AMCW), which works by modulating the optical power continuously and measuring distance based on the phase difference between the received signal and a reference within an integration window. This method shares conceptual similarities with pulsed ToF, but employs a continuous wave approach [1]. Furthermore, the Frequency Modulated Continuous Wave (FMCW) method measures distance based on the frequency difference resulting from the time-of-flight delay between the emitted and reflected laser signals [9].

The time-of-flight (ToF) method offers broad application potential. In this method, an active light source is directed toward a target surface, and the distance to the object is determined by calculating the round-trip time of the reflected signal. This method is relatively straightforward to implement and allows for simpler and more cost-effective system design. The basic ToF method can be categorized into Direct Time of Flight (d-ToF) and Indirect Time of Flight (iToF). LiDAR sensors employing the i-ToF method offer advantages and potential for highresolution short-range applications such as facial recognition and augmented reality (AR) [10]. To acquire 3D information of an object, LiDAR systems require a scanning mechanism. This mechanism plays a crucial role as it significantly influences the overall system design. LiDAR scanning systems are generally classified into four main categories: opto-mechanical, electromechanical, MEMS-based, and solid-state systems [11]. System evaluation typically involves parameters such as wavelength, transmitted power, detection range, field of view (FoV), precision, accuracy, resolution, and scan rate [12]. LiDAR systems commonly operate at two main wavelengths: 905 nm and 1550 nm [13][14]. Laser sources with a wavelength of 1550 nm demonstrate superior performance compared to those operating at 905 nm, particularly in terms of detection range and eye safety. This advantage is based on the property of wavelengths above 1400 nm being absorbed by the anterior layers of the eye, thereby preventing the beam from reaching the retina and allowing higher transmission power to be used safely [14]. To date, most research

involving 1550 nm lasers has focused on the Frequency Modulated Continuous Wave (FMCW) method [13].

In this study, the authors developed a 1550 nm LiDAR system using the Indirect Time of Flight (i-ToF) method and applied a 5 V sinusoidal modulation at 100 MHz to the laser diode source. Distance is measured based on the phase difference between the modulated signal and the reflected signal received from the object. To support scanning, a galvanometer model GVS002 is utilized, classified as an opto-mechanical scanning mechanism. The GVS002 system employs a dual-mirror galvanometer configuration, enabling precise two-dimensional scanning across object surfaces. The novelty of this system lies in its application of LiDAR for accurate spatial mapping at short ranges, which often poses challenges in conventional LiDAR systems. By employing stable amplitude-modulated continuous waves and high frequency modulation, the system enhances sensitivity to small variations in distance, making it well suited for detecting small sized objects.

2. Method

2.1 Theorical Background

Light Detection and Ranging (LiDAR) is an optical distance measurement technology that utilizes the principle of laser light reflection to obtain distance information with high precision. LiDAR operates by emitting a laser signal toward an object and subsequently detecting the reflected signal that returns to the receiving system.

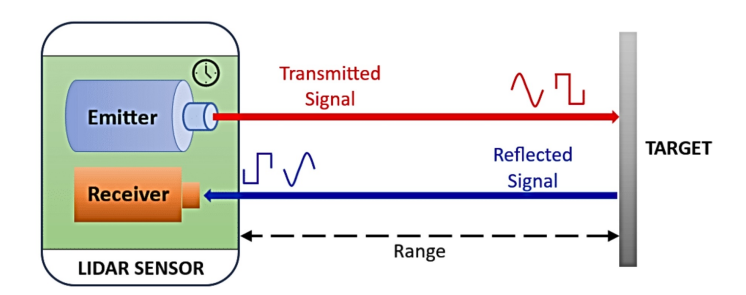


Figure 1. The working principle of LiDAR

In Figure 1, the working principle of LiDAR involves emitting light from a transmitter toward a target object, after which the reflected light is received by a receiver (photodetector). The distance can be calculated by measuring the time-of-flight of the light, using Equation (1) [15]:

$$R(Range) = \frac{1}{2}c\tau \tag{1}$$

where c is the speed of light (3 × 10⁸ m/s), and τ denotes the round-trip travel time. Indirect Time of Flight (i-ToF) is a distance measurement method in LiDAR systems that utilizes a continuously modulated light signal, typically in the form of a sinusoidal waveform. According to Equation (1), the round-trip travel time is represented by τ . In this study, the researchers employed frequency modulation to determine the value

570

of τ . The object distance is represented by the phase difference between the modulated waveform and the reflected waveform, as described by the following equation:

$$d = \frac{c}{2f_M} \frac{\Delta \varphi}{360^{\circ}} \tag{2}$$

where d is the distance to the object, = 3×10^8 m/s is the speed of light, $\Delta \phi$ is the phase difference and f_M is the modulation frequency.

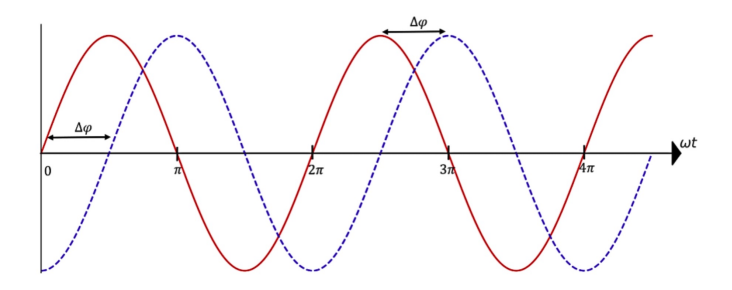


Figure 2. Phase difference of transmitted (-) and reflected (—) waves

Figure 2 shows the phase difference $\Delta \phi$ between the transmitted signal waveform and the reflected or return signal. According to Equation (2), the phase difference is limited to the range of (0, 360°). The maximum measurable distance depends on the modulation frequency used. If the detected object lies beyond the measurable range, a phenomenon known as distance ambiguity will occur [15]. This distance ambiguity (du) can be determined using the following equation:

$$du = \frac{c}{2f_M} \tag{3}$$

Table 1 presents the calculated maximum measurable distances and resolution per 1° for several possible modulation frequency variations: 1 MHz, 10 MHz, 50 MHz, 100 MHz, to 200 MHz.

Modulation Frequency	Maximum Distance	Resolution ($\Delta \phi = 1^{\circ}$)
(MHz)	(m)	(mm)
1	150	420
10	15	42
50	3	8.3
100	1.5	4.2
200	0.75	2.1

Table 1. Distance and resolution of i-ToF LiDAR based on modulation frequency

Table 1 shows the relationship between modulation frequency and the performance of a LiDAR system based on the indirect Time-of-Flight (i-ToF) method. It can be observed that higher modulation frequencies result in better distance measurement

resolution (indicated by a decrease in resolution values in millimeters). However, this improvement in resolution comes at the cost of a reduced maximum detection range.

2.2 Scanning Mechanisms

LiDAR systems can acquire distance information in 1D, 2D, and 3D. For 2D and 3D data acquisition, a scanning mechanism is required, which significantly influences the overall system design. This study employs a galvanometer (GVS002), which belongs to the opto-mechanical scanning category and utilizes mirrors to steer the light beam.

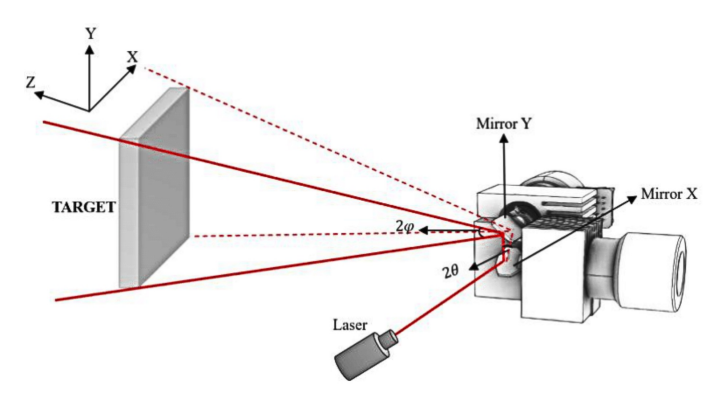


Figure 3. Galvanometer optical scanning mechanism

Figure 3 illustrates the working mechanism of a galvanometer. The galvanometer consists of two mirrors, each driven by vibrations or motor rotation. Initially, the light beam strikes the X-axis mirror, resulting in a reflection angle of 2θ degrees. It is then reflected onto the Y-axis mirror, forming a reflection angle of 2ϕ degrees. The angles θ and ϕ represent the optical scan angles, which depend on the amount of voltage applied to the motors (mechanical scan angles). The mechanical scan angles can be determined using Equation (4) and Equation (5):

$$\Theta_{mech} = k \times V_x \tag{4}$$

$$\varphi_{mech} = -k \times V_{\gamma} \tag{5}$$

where θ_{mech} is the mechanical scan angle of the X-axis mirror, ϕ_{mech} is the mechanical scan angle of the Y-axis mirror. V_X is the input voltage to the motor driving the X-axis mirror, V_Y the input voltage to the motor driving the Y-axis mirror, and k is the galvanometer conversion constant (°/V). The relationship between the mechanical scan angles and the optical scan angles is defined by Equation (6) and Equation (7):

$$\theta = 2 \times \theta_{mech} \tag{6}$$

$$\varphi = 2 \times \varphi_{mech} \tag{7}$$

Under balanced or neutral conditions, the voltage applied to both the X-axis and Y-axis motors is 0 V. In this state, the laser beam will be positioned at the neutral coordinate (X = 0, Y = 0).

2.3 3D Point Cloud

3D point cloud is a three-dimensional spatial representation consisting of a set of discrete points in the coordinate space (X, Y, Z). The X coordinate represents the left-right position, Y represents the vertical (up-down) position, and Z represents the depth or the distance from the sensor to the target. Each coordinate value is determined based on the following equations:

$$X = r.sin(\theta) \tag{8}$$

$$Y = r.sin(\varphi) \tag{9}$$

$$Z = r.cos(\varphi).cos(\theta) \tag{10}$$

r is the distance obtained from Equation (2) using the indirect Time-of-Flight (i-ToF) method. 2.4 Experimental Setup

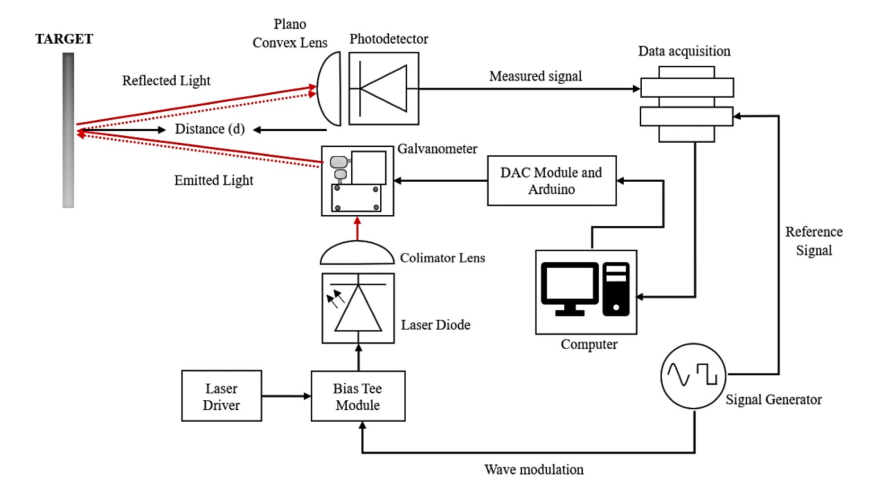


Figure 4. The schematic of LiDAR system with i-ToF method

Figure 4 shows how the LiDAR system flow with the i-ToF method works. The process begins by activating the laser driver with a current setting of 150 mA which will produce an optical power of 22,210 mW. The current is then directed to a Bias Tee module, which functions to combine the DC signal from the laser driver with a high-frequency AC signal from the signal generator. The AC signal is a sinusoidal waveform with a frequency of 100 MHz and a voltage of 5 Vpp, serving as the modulation signal. The output from the Bias Tee module results in modulated infrared light with a wavelength of 1550 nm, which is then delivered to the laser diode (LDM9LP). The laser light generated by the diode is collimated through a collimator lens, producing a parallel beam. The collimator lens plays a crucial role in reducing divergence to ensure that the beam remains focused as it is directed toward the mirrors in the galvanometer. The reflection angles on the X and Y galvanometer mirrors are controlled by a DAC module (AD5689) and an Arduino-based system, which receives control signals from a computer.

Through the galvanometer, the laser beam strikes the surface of the target, which consists of a plate covered with aluminum foil having a reflectance factor of approximately 80–90%. The reflected light is then directed toward a photodetector through a plano-concave lens. The photodetector transmits the measurement signal to the Picoscope module (Picoscope 2208b), which serves as the data acquisition (DAQ) module. The Picoscope also receives a reference signal with identical characteristics to the modulation signal generated by the signal generator. The DAQ system then measures the phase difference between the two signals. This phase difference is used to calculate the distance between the system and the target point based on Equation (3). The computer subsequently processes the measurement results for each scan point and compiles the coordinate data (X, Y, Z) into a point cloud based on Equations (8–10), representing the surface of the object in three dimensions.

3. Result and Analysis

3.1 Alignment and Central Point Testing

This experiment was conducted to verify that the galvanometer and laser system were properly and accurately aligned when positioned at the center (X = 0 V) and Y = 0V). This test is critical to perform at the beginning of the experiment, as this central position serves as the reference coordinate system for the entire scanning process. Any misalignment at this point may result in a systematic shift across the entire 3D scan, thereby reducing mapping accuracy. For this purpose, millimeter graph paper was used as a visual reference plane. The experiment was carried out by placing the target at various distances: 5 cm, 10 cm, 20 cm, 30 cm, and up to 100 cm. Observations were then made on the position of the laser beam to ensure that it remained aligned along a straight line. The results showed that the laser beam remained fixed on a single point up to a distance of 70 cm from the system. At distances beyond 70 cm, slight angular deviations were observed, although they did not exceed 1 mm. However, such deviations remained within the limits of visual observation tolerance. Through this experiment, it was confirmed that the collimator lens effectively maintained beam sharpness and consistency across varying distances, resulting in consistent beam visibility and minimal divergence.

3.2 Galvanometer Voltage Response

This experiment was conducted to observe how the galvanometer responds to variations in input voltage supplied through the DAC, and to evaluate the accuracy and consistency of the galvanometer's angular deviation in steering the laser beam onto the target surface. This assessment is crucial, as the galvanometer's response directly affects the final coordinates (X, Y, Z) in the resulting 3D point cloud. The galvanometer used in this study has an input voltage sensitivity (k) 0,8 V per 1° of mechanical scan angle and 2° of optical scan angle, as defined in Equations (6) and Equations (7). Input voltage was gradually applied to the X-axis and Y-axis motors, ranging from – 4 V to +4 V. The experiment was performed at a fixed distance of 30 cm between the galvanometer and the target surface, which was covered with millimeter graph paper to facilitate visual observation of the reflected beam position. Using Equation (8) for

the X-axis and Equation (9) for the Y-axis, it was demonstrated that voltage variation directly influences the laser beam position on the target surface.

The GVS202 galvanometer exhibits asymmetric reflection behavior between the X and Y mirrors. When a positive voltage (+V) is applied to the X mirror, the laser beam deflects to the right (positive horizontal direction), whereas a negative voltage (-V) causes deflection to the left (negative horizontal direction). Conversely, applying a positive voltage (+V) to the Y mirror causes the beam to deflect downward (negative vertical direction), while a negative voltage (-V) causes upward deflection (positive vertical direction).

Figure 5 shows a linear relationship between the input voltage applied to the X-axis galvanometer and the resulting horizontal position of the laser beam on the target. The beam position increases proportionally with input voltage, ranging from – 53 mm to +53 mm as the voltage changes from – 4 V to +4 V. Meanwhile, Figure 6 shows the response of the Y-axis galvanometer, which exhibits an inverse linear relationship with the input voltage. The vertical beam position ranges from +53 mm to –53 mm for input voltages from – 4 V to +4 V, indicating that the system gain magnitude is equivalent but has opposite sign.

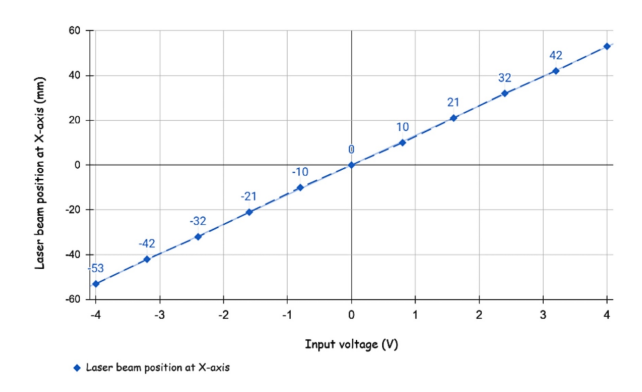


Figure 5. Laser beam displacement on the target along the X-axis

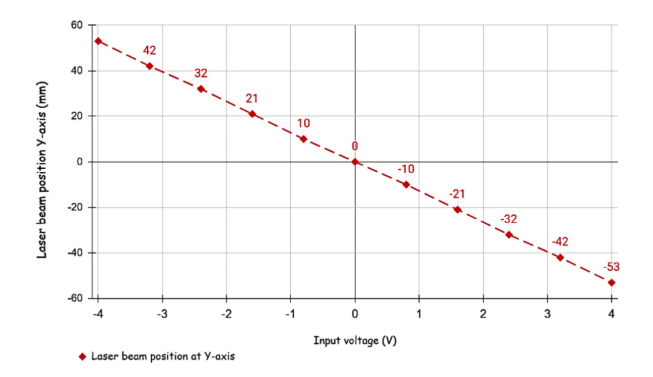


Figure 6. Laser beam displacement on the target along the Y-axis

3.3 System Resolution and System Calibration

At this stage, the researcher conducted tests by comparing the system measurements with measurements using the BOSCH GLM 40 laser distance, with the angle conditions φ and θ on the galvanometer scanner set to 0°. In other words, this test places the system in a mode to measure distance only (range finder). This is done to test whether the system calibration matches the already calibrated measuring instrument. And to see how the linearity of the system works. In this research, sinusoidal wave modulation at a frequency of 100 MHz was used. The measurement resolution that can be detected by the data acquisition system is 0.01° using the Picoscope 2208B. Based on Equation (2), it can be calculated that the theoretical resolution of the system is 4.2 mm/1 ° $\Delta \varphi$, so with a measurement resolution of 0.01 °, the system can detect a distance difference of 0.042 mm. The calculation of the target distance limit can be determined using Equation (3). Based on these calculations, it is found that the system can only measure distances up to 1.5 m before phase repetition occurs, known as the range ambiguity phenomenon. If the target distance exceeds 1.5 m, the system will calculate the phase value as if the target were in the next cycle, requiring system enhancement such as the use of dual frequency (dual frequency i-ToF). Based on Table 1, it is shown that high-resolution measurements can be obtained by using a higher frequency. The measurements were taken by changing the object distance by 1.00 cm based on the reference with the BOSCH GLM40 laser distance meter. Figure 7 shows the phase difference measurement results for five trials with the linear equation y = 0.241x - 0.2302. The graph of the relationship between the actual distance from the sensor and the measured phase difference shows a linear and consistent trend throughout the experiment, with an average accuracy of MAE (0.06913 cm), RMSE (0.09091 cm), and average standard deviation or STD (0.07865 cm). This indicates that the system has high accuracy and fairly good measurement stability. This data is also important to support the development of error correction algorithms or confidence mapping in phase difference-based LiDAR systems.

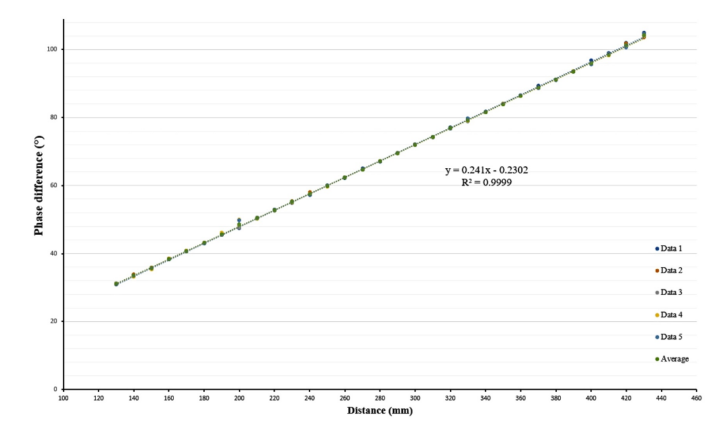


Figure 7. Phase difference measurement results with respect to distance variation

3.4 Surface Reconstruction Result

In this section, the researchers conducted measurements on a flat surface (plate) using the developed LiDAR system. The system employed a fixed angular step of 1°, with a horizontal angle range (θ) from – 2° to +2° and a vertical angle range (ϕ) from – 2° to +4°, resulting in a 3D point cloud distributed in a 5 × 7 grid, comprising a total of 35 points. The laser spot used had a size of 4 mm × 4 mm, and the target was placed at two different distances: 25 cm (Figure 8a) and 35 cm (Figure 8b) from the sensor. The angular ranges of θ and ϕ are determined by the active area of the photodetector.

The measurement results (Figure 9) indicate that the object surface can be accurately mapped, with Z-coordinate values remaining relatively consistent, approximating a flat plane. At a distance of 25 cm, the point distribution covered an area of approximately 1.76 cm × 2.63 cm, with an average point spacing of about 0.436 cm. At 35 cm, the coverage area increased to 2.45 cm × 3.66 cm, while the point spacing also increased to approximately 0.611 cm. This demonstrates that, under constant angular steps, increasing the measurement distance leads to a larger coverage area but at the cost of reduced spatial resolution. Furthermore, the point cloud results show good stability along the Z-axis, indicating a relatively consistent flat surface. However, several points exhibited significant deviations along the Z-axis, with one point measuring 25.28 cm noticeably different from the average value of 25.00 cm. These outlier points were located at extreme angles ($\theta = -2^{\circ}, \varphi = -2^{\circ}$), which were likely affected by reflected signal noise, phase measurement errors, or misalignment between the reflected beam and the photodetector. This finding highlights the importance of calibrating both the optical and electrical components of the system to minimize measurement errors at angular extremes. Overall, the experiment demonstrates that the LiDAR system is capable of effectively mapping flat surfaces at both measured distances, although spatial resolution tends to decrease with increased target distance.

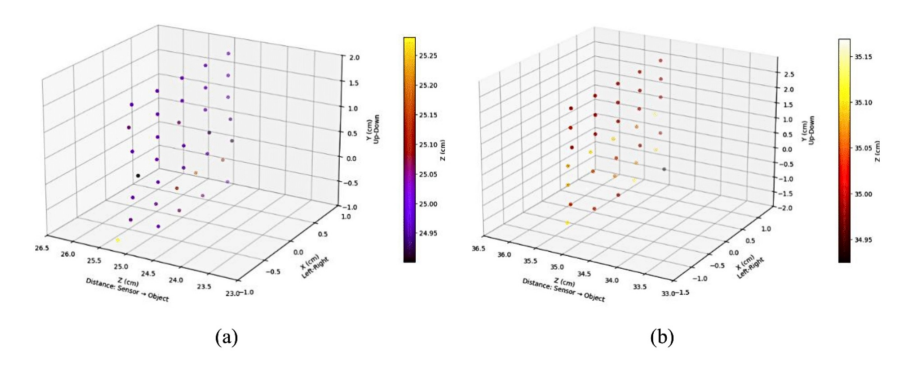


Figure 8. 3D Point cloud data of the plate surface at distances: (a) 25 cm, (b) 35 cm

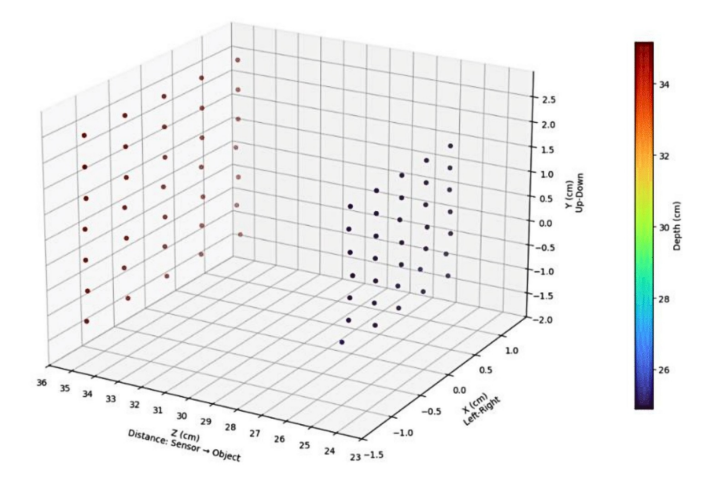


Figure 9. 3D point cloud data of the plate surface at 25 cm and 35 cm distances

4. Conclusion

Based on the experiments conducted, the galvanometer-based LiDAR system demonstrated optical stability up to a distance of 70 cm under a modulation frequency of 100 MHz. Additionally, the galvanometer's response to varying input voltages showed a consistent linear relationship with the movement of the laser beam. The i-ToF method also proved to produce linear and stable distance measurements, although it is limited to a maximum range of 1.5 m due to the 360° phase difference constraint. When the distance exceeds 1.5 m, ambiguous phase differences occur. The results of the plate dimension measurements at 25 cm (1.76 cm × 2.63 cm) and 35 cm (2.45 cm × 3.66 cm) indicate that increasing the object distance from the system leads to a wider coverage area, but with a reduction in spatial resolution. At a distance of 25 cm the spatial resolution is 0.436 cm, and at a distance of 35 cm, the spatial resolution is 0.611 cm. This LiDAR system configuration produces linear and stable distance measurements under ideal conditions (galvanometer scanner reflection angle of 0°). A 1° phase difference change represents 4.2 mm (0.42 cm). With a Mean Absolute Error (MAE) of 0.06913 cm, Root Mean Squared Error (RMSE) of 0.09091 cm, and an average standard deviation (STD) of 0.07865 cm.

Acknowledgement

The authors would like to acknowledge Fajar Saputra, a fellow internship student who conducted joint research at BRIN.

References

- R. Roriz, J. Cabral, and T. Gomes. "Automotive LiDAR technology: A survey". In: IEEE Trans. Intell. Transp. Syst. 23.7 (July 2022), pp. 6282–6297.
- [2] T.-H. Kim and T.-H. Park. "Placement optimization of multiple LiDAR sensors for autonomous vehicles". In: IEEE Trans. Intell. Transp. Syst. 21.5 (May 2020), pp. 2139–2145.

- [3] S. Royo and M. Ballesta-Garcia. "An overview of LiDAR imaging systems for autonomous vehicles". In: Appl. Sci. 9.19 (Sept. 2019), p. 4093.
- [4] P. Seoane et al. "Assessment of LiDAR-based sensing technologies in bird-drone collision scenarios". In: Drones 9 (2025), p. 13.
- [5] Z. Miao et al. "Drone LiDAR occlusion analysis and simulation". In: Drones 9.2 (2025), p. 135.
- [6] G. Mandlburger and B. Jutzi. "On the feasibility of water surface mapping with single photon LiDAR". In: ISPRS Int. J. Geo-Inf. 8.4 (Apr. 2019), p. 188.
- [7] J. H. Churnside and J. A. Shaw. "LiDAR remote sensing of the aquatic environment". In: Appl. Opt. 59.10 (Apr. 2020), p. C92.
- [8] F. Wang et al. "Design and implementation of the galvanometer scanning system". In: Chin. Opt. Lett. 18.12 (2020), p. 121703.
- [9] T. Staffas et al. "FMCW and ToF LiDAR with single photons: A comparison". In: Opt. Express 32.5 (Feb. 2024), pp. 7332–7341.
- [10] Y. Xin et al. "A low-power i-ToF LiDAR with nonlinearity self-calibration technique". In: IEEE Trans. Instrum. Meas. 72 (2023).
- [11] T. Raj et al. "A survey on LiDAR scanning mechanisms". In: Electronics 9.5 (2020), p. 741.
- [12] J. Lambert et al. "Performance analysis of 3D LiDARs for automated driving". In: *IEEE Access* 8 (2020), pp. 131699–131722.
- [13] C. Rablau. "LiDAR: A new self-driving vehicle for introducing optics to broader engineering and non-engineering audiences". In: *Proc. 15th Conf. Educ. Training Opt. Photon. (ETOP)*. Vol. 11143. 2022.
- [14] J. Wojtanowski et al. "Comparison of 905 nm and 1550 nm semiconductor laser rangefinders". In: Opto-Electron. Rev. 22.3 (2014), pp. 183–190.
- [15] D. Hanto et al. "ToF LiDAR with dual-modulation frequency switching". In: IEEE Trans. Instrum. Meas. 72 (2023).